Femtochemistry of mass-selected negative-ion clusters of dioxygen: Charge-transfer and solvation dynamics

D. Hern Paik, Thorsten M. Bernhardt, Nam Joon Kim, and Ahmed H. Zewail

Citation: The Journal of Chemical Physics **115**, 612 (2001); doi: 10.1063/1.1384549
View online: http://dx.doi.org/10.1063/1.1384549
View Table of Contents: http://scitation.aip.org/content/aip/journal/jcp/115/2?ver=pdfcov
Published by the AIP Publishing

Femtochemistry of mass-selected negative-ion clusters of dioxygen: Charge-transfer and solvation dynamics

D. Hern Paik, Thorsten M. Bernhardt,[a] Nam Joon Kim, and Ahmed H. Zewail[b]
Arthur Amos Noyes Laboratory of Chemical Physics, Laboratory for Molecular Sciences, California Institute of Technology, Pasadena, California 91125

(Received 28 March 2001; accepted 17 May 2001)

Femtosecond, time-resolved photoelectron spectroscopy is used to investigate the dissociation dynamics of mass-selected anionic molecular-oxygen clusters. The observed transient photoelectron signal for the clusters $(O_2)_n^-$ $(n=3-5)$ shows the O_2^- production; for $n=1$ and 2, we observe no time-dependence at this wavelength of 800 nm. The observed transients are bi-exponential in form with two distinct time constants, but with clear trends, for all investigated cluster sizes. These striking observations describe the reaction pathways of the solvated core and we elucidate two primary processes: Charge transfer with concomitant nuclear motion, and direct dissociation of the O_4^- core-ion via electron recombination; the former takes 700–2700 fs, while the latter is on a shorter time scale, 110–420 fs. Both rates decrease differently upon increasing cluster size, indicating the critical role of step-wise solvation. © *2001 American Institute of Physics.*
[DOI: 10.1063/1.1384549]

I. INTRODUCTION

Spectroscopy of size-selected molecular clusters provides a unique approach to investigate solvation phenomena at the molecular level; for recent reviews see Refs. 1–3. For ions, mass selection provides an opportunity to study the energetics and dynamics, with the solvent number of atoms or molecules being well-defined. Homogeneous ionic clusters are of particular interest as they could exhibit unique features of electron and energy transfer, and solvation. For example, in a number of ionic cluster systems, such as $(CO_2)_n^-$, a dimeric core unit is found to be responsible for the observed photochemistry.[4] In some other examples, such as Ar_n^+ and $(H_2O)_n^-$, photoexcitation can lead to a charge-transfer to neutral solvent molecules, as shown by the Johnson group.[5,6]

The relevant homogeneous system here is the anionic molecular-oxygen clusters studied by the groups of Johnson, Continetti, Märk, and others.[7–9] The O_4^- chromophore is suggested to be the core unit,[10] which is transparent in the near-infrared region. However, with the addition of O_2 solvent molecules to the O_4^- core, cluster dissociation occurs upon infrared absorption.[11] Two mechanisms are proposed in the literature to account for the observed photodissociation of $(O_2)_n^-$ clusters: (i) Near-infrared excitation to a charge-transfer state which involves O_4^- and the solvent.[11] Following this charge transfer, the newly generated O_2^- ion exhibits a significant vibrational excitation, which by cooling leads to sequential evaporation of neutral O_2 molecules.[12] (ii) Excitation to low-lying repulsive states, which are not accessible in native O_4^-, but become possible in the larger $(O_2)_n^-$ $(n>2)$ clusters.[8] In this case, vibrational excitation of product O_2^- can also be observed. However, the time scale for the O_2^- release in these two mechanisms has to differ considerably.

In this contribution, we report, using femtosecond photoelectron (PE) spectroscopy, study of the dissociation dynamics in real time of mass-selected clusters of molecular oxygen. The method is capable of resolving the femtosecond dynamics of ions with mass selection as a function of size.[13,14] For our study of $(O_2)_n^-$ clusters in the newly designed molecular beam machine, described here briefly, we identify two distinct dissociation channels which occur on drastically different time scales. We conclude that the preparation of the charge-transfer complex leads to the bifurcation of the wave packet, with liberation of the charge-accepted O_2^- in one channel and electron recombination which leads to O_4^- in the second channel. This second process is analogous to previous investigations of bimolecular charge-transfer reactions in neutral van der Waals clusters, which revealed the importance of reversible electron transfer.[15,16] The influence of stepwise solvation by O_2 on the reaction timescale is also observed and is consistent with the aforementioned picture.

II. EXPERIMENT

A schematic representation of the molecular beam apparatus is illustrated in Fig. 1. The full description will be given elsewhere (Thorsten M. Berhnardt and D. Hern Paik, work to be published for this laboratory). Here we provide a brief discussion. Anionic oxygen clusters were generated by secondary electron attachment after the supersonic expansion. The anionic clusters were extracted to the field-free time-of-flight region by a pulsed electric field. A particular size was selected by an interleaved-comb massgate[17] before entering the interaction-with-light region. The clusters of interest were then perpendicularly intercepted with femtosecond laser pulses, which produces photofragments and photoelec-

[a]Permanent address: Institut für Experimentalphysik, Freie Universität Berlin, Arnimallee 14, D-14195 Berlin, Germany.
[b]Electronic mail: zewail@caltech.edu

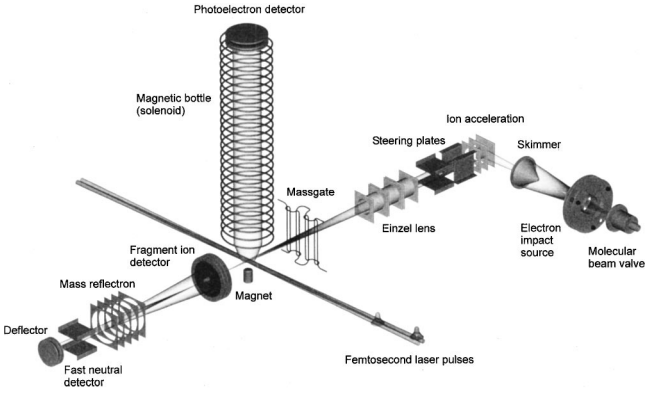

FIG. 1. Schematic representation of the experimental setup, highlighting details of the newly-built apparatus (see the text).

trons. The nascent fragment ions were separated in time from the parent ions after reflection from the linear reflectron. The linear configuration of a reflectron provides the minimal deviation of the daughter-ion trajectories from the parent ions, which facilitate the analysis of the dissociation process by incorporating the relative intensity profiles of ion signals.[18] Photoelectrons were analyzed using a magnetic-bottle photoelectron spectrometer (76 cm length).[19,20] Here, no decelerating field was applied to slow down the ion beam. Consequently, the resolution of the spectrometer is limited to 150–200 meV at 1 eV electron kinetic energy due to Doppler broadening.

Intense femtosecond laser pulses (100 fs, 800 nm, 25 mJ/pulse, 20 Hz) were generated using a Ti:sapphire regenerative amplifier which is seeded with the output of a Ti:sapphire oscillator and pumped by the second harmonic (532 nm) of two Nd:YAG lasers. Twenty percent of the output power was used in these experiments to produce the 800 nm pump pulse with about 1.5 mJ and the 400 nm probe pulse (second harmonic generation using a BBO crystal) with 0.8 mJ before the entrance window. Pump and probe pulses were colinearly directed into the molecular beam chamber, and the beam diameters of both were collimated to ~5 mm in order to achieve optimal overlap with the ion beam, minimizing multiphoton processes. We monitored the transients in real time by probing the time-dependent photoelectron spectrum of the nascent O_2^- fragment. We also studied the decay of the parent, which appears as a transient signal with a decay time constant.

III. RESULTS

A mass spectrum of $(O_2)_n^-$ generated by the cluster ion source (no laser) is shown in Fig. 2(a). With 800 nm fs pulse, the fragment mass spectra of $(O_2)_n^-$ $(n=3-5)$ are displayed in Fig. 2(b). The irradiation of O_2^- and O_4^- with 800 nm pulse did not produce any detectable negatively-charged fragments. The mass spectra of Fig. 2(b) clearly indicate that the major anionic product of the $(O_2)_n^-$ $(n=3-5)$ dissociation is the O_2^- fragment. Moreover, the intensity distribution shows the growth of the O_4^- fragment with increasing cluster size. These results are in good agreement with previous photodissociation studies of $(O_2)_n^-$ at 1064 nm excitation.[11]

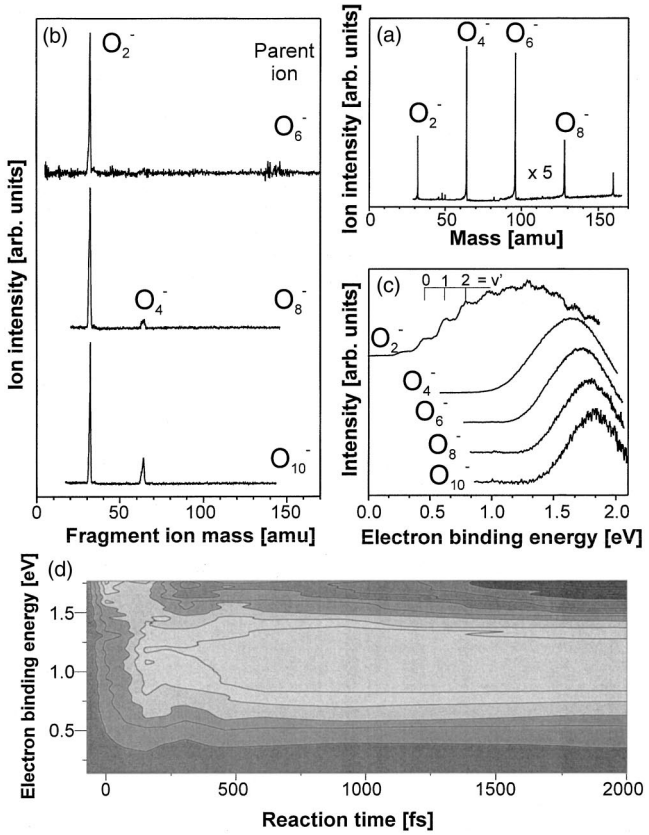

FIG. 2. (a) Mass spectrum of anionic oxygen clusters generated by the ion source. (b) Fragment ion mass spectra recorded utilizing the linear reflectron mass spectrometer. The parent cluster size of the corresponding fragment spectrum is indicated on the right of each trace. (c) Photoelectron spectra at 3.1 eV laser energy (400 nm) of all investigated $(O_2)_n^-$ clusters. The vibrational progression indicated in the O_2^- photoelectron spectrum originates from the $O_2\,X\,^3\Sigma_g^-(v')\leftarrow O_2^-\,^2\Pi_g(v''=0)$ transition (Ref. 11). (d) Two-dimensional contour plot of the time-dependent photoelectron spectrum of the nascent O_2^- generated from the O_{10}^- dissociation, $O_{10}^-\rightarrow O_2^-+4O_2$. In the contour plot, the intensity profile is indicated by the gray scale: The bright gray region in the contour plot corresponds to the positive envelope of the photoelectron spectrum, while the dark gray region indicates the negative envelope. Note that the contour is constructed from the total time-dependent signal, (pump+probe) minus that of the reference (pump+probe) at $t=0$.

Figure 2(c) shows the photoelectron spectra of $(O_2)_n^-$ clusters recorded at 400 nm (3.1 eV) probe irradiation. The photodetachment spectra of $(O_2)_n^-$ at this wavelength are similar to the previously reported spectra at 532 nm,[8] 355 nm,[8,11] and 266 nm.[8] The onset of the photoelectron spectrum (adiabatic electron affinity) of O_4^- is 0.5 eV shifted to higher electron binding energy with respect to the O_2^- PE spectrum, while ~0.1 eV shift is observed upon increasing the cluster size. Aside from the shifts, the shapes of the PE spectra of $(O_2)_n^-$ $(n=3-5)$ resemble that of O_4^-. These results, as with previous studies of thermochemical data,[10] photoelectron spectroscopy[11] and matrix isolation,[21] are consistent with the structure of the core being O_4^- solvated with neutral O_2 molecules.

The bottom panel in Fig. 2 shows a two-dimensional (2-D) representation of the change in time of the electron binding energy (BE): The photon energy $(h\nu)=\mathrm{BE}+\mathrm{KE}$ (kinetic energy). For all BEs, the temporal behavior is similar, displaying two distinct time scales; at lower BE, the behavior

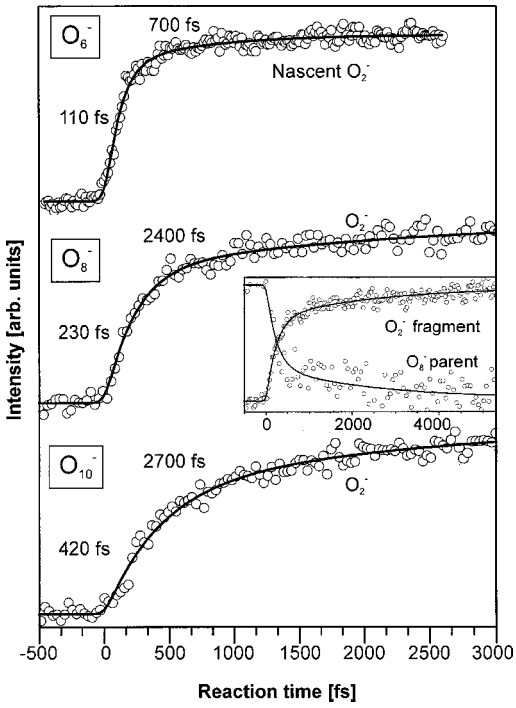

FIG. 3. Femtosecond transients of the $(O_2)_n^-$ photodissociation reaction at 800 nm excitation. Shown are the changes of the nascent O_2^- photoelectron signal as a function of the delay time between pump and probe laser pulses. We also display the parent ion decay signal as an inset for the case of O_8^- in order to compare with the product signal growth. All transient data are well fitted by a bi-exponential function, and the error bars are typically ± 50 fs for the fast component and ± 200 fs (for O_6^-) to ± 500 fs (for O_{10}^-) for the slow component. Note that the signal depicts a rise and any autodetachment of O_2^- to O_2 would appear as a decay at long times (see Ref. 22); the threshold is at $v''=4$ of O_2^- and our O_2^- photoelectron spectra terminates near $v''=3$, confirming negligible population for the observation of autodetachment.

is that of a bi-exponential rise, while at higher BE, it becomes more of a decay transient due to the shift of the PE with size [see Fig. 2(c)]. We also recorded the entire PE spectra for O_6^-, O_8^- and O_{10}^- as a function of time (not shown). We clearly see the increase of the envelope intensity upon going to longer delay times, and the envelope is in the energy range of O_2^-, consistent with its direct production. The O_2^- is vibrationally-excited, especially from O_6^-, in agreement with previous nanosecond work.[12]

The femtosecond transients of nascent O_2^- and the parent ion are shown in Fig. 3. The transient was recorded by gating either at the positive intensity envelope of O_2^- (build-up) or at the negative intensity signal of the parent $(O_2)_n^-$ (decay). Care was taken to exclude possible contributions of O_4^- fragments in the case of O_8^- and O_{10}^- by adjusting the position of the gate. All transients, including the decay of the parent (O_8^-), exhibit two distinct exponential components. The time constants differ by a factor of 6–10, and both time constants increase as the cluster size increases.

To quantify the analysis we fitted the data to a bi-exponential rise (or the parent decay), varying the amplitudes (A_1 and A_2) and time constants (τ_1 and τ_2); the response function, using the autocorrelation pulse measurement (FWHM: 100 ± 5 fs), was also included. The results are shown in Fig. 3: For O_6^-, $\tau_1=110$ fs, $\tau_2=700$ fs, γ $(\equiv A_1/A_2)=4$; for O_8^-, $\tau_1=230$ fs, $\tau_2=2400$ fs, $\gamma=2.7$; for O_{10}^-, $\tau_1=420$ fs, $\tau_2=2700$ fs, $\gamma=1.65$.

Based on studies of the power dependence of the pump pulse, the possibility of multiphoton processes was excluded because of the following: First, we observed a slope of ~ 0.5 in the plot of log(signal) vs log(I_{pump}), consistent with previous nanosecond work,[11] indicating a one-photon absorption (linear) and one-photon absorption/one-photon depletion by the same 800 nm wavelength; if two 800 nm pump photons are involved in the dissociation of the cluster (followed by 400 nm probe photodetachment of O_2^-), then the slope will be $\geqslant 1$, maximum 2. Second, we also recorded the transient behavior at half the pump power and observed the same transients. Third, if the fast component is due to two pump photons to the higher-energy repulsive potential, we do not expect the dramatic change observed for the rates of O_6^-, O_8^- and O_{10}^-. Accordingly, the transient signal reported here is for a one-photon excitation at 800 nm, followed by a one-photon detachment at 400 nm (generated by SHG).

IV. DISCUSSION

The temporal behavior (with energy resolution) and the observed trends for the three solvated species, O_6^-, O_8^- and O_{10}^-, elucidate the presence of two pathways in the mechanism of cluster-ion fragmentation and solvent evaporation. The equilibrium structure of these clusters is not known, but experimental[11,12] and *ab initio*[23] calculations indicate that a core O_4^- is involved as a building block with solvation by neutral O_2 increasing as the cluster size increases. In O_6^- and larger clusters it has been shown by the Johnson's group that charge-transfer takes place, and in these clusters they observed photodissociation following infrared excitation at 1064 nm; since the spectrum of O_4^- and O_2^- do not show absorption in this region, the behavior is consistent with a charge-transfer excitation.

The femtosecond excitation launches a wave packet in all of nuclear space. We only consider the relevant nuclear coordinates shown in Fig. 4, for O_6^-. These are the O_2-O_2 separations of O_4^- and the O_2^- separation from O_4. The bifurcation of the wave packet is considered following the initial preparation from the strongly bound O_4^- core to O_2. The influence of solvation by additional O_2 molecules on the nuclear motion is illustrated by the caging barrier, schematically presented in Fig. 4 at a long O_2-O_2 distance.

Upon femtosecond excitation, electron transfer (ET) from the O_4^- core to the O_2 solvent occurs, with O_2^- vibrationally excited (see Sec. III). This state of O_2^- can relax, either via autodetachment to form ground-state $O_2(O_2^- \rightarrow O_2 + e^-)$ or via coupling with O_4, now-neutral core[8,11,24] the autodetachment channel will not give a time-dependent rising signal as no photodetachment of O_2 will be possible. Thus the observed transient in this channel reflects the dynamics of O_2^- liberation. The importance of electron recombination (ER) has been recognized before in femtosecond dynamics of charge-transfer reactions.[15,16] After charge-transfer excitation, back electron transfer to the O_4 core populates the excited complex onto a repulsive state which is

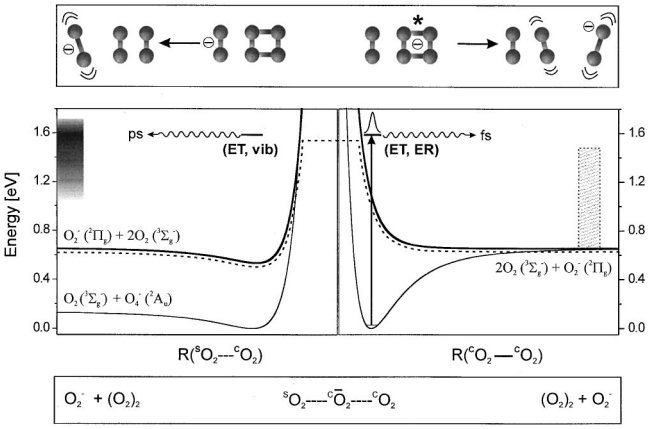

FIG. 4. A representation of two cuts in the O_6^- potential energy surface. On the left hand side of the figure, the potential is along the nuclear coordinate between the solvent O_2^- and core $O_4(^SO_2\cdots{}^CO_2)$; charge induced–dipole interaction. On the right hand side, the potential for the separation ($^CO_2$-$^CO_2$) of O_2^- from O_2 in core O_4^- is displayed; the solvent neutral O_2 is considered as a spectator, thus the dissociation energy of O_6^- (0.63 eV) is plotted in the asymptote even though O_4^- dissociation energy is 0.52 eV (Ref. 11). Note that the reaction in the box at the bottom implies symmetry along the dotted potential path, but because of the stability of O_4^- in contrast with O_4 there is some asymmetry (see Refs. 8 and 23 for theoretical *ab initio* calculations). The hatched area in this panel represents the solvent barrier responsible for caging. The wave packet is launched as indicated, and the bifurcation is illustrated by the dotted path. The estimated energy range of the charge transfer band is shown on the energy axis to the left; the width is determined by the range between the adiabatic electron affinity and vertical detachment energy of O_6^-, similar to estimates made for other systems (Ref. 5).

not directly accessible by optical excitation in O_4^- at this wavelength. This repulsion leads to direct dissociation of the O_4^- core ion and the wave packet rapidly enters the region where the photodetachment signal of O_2^- is produced in 110 fs for O_6^-. This reaction path is depicted on the right hand side of Fig. 4.

The other trajectories of the dynamics result from the bifurcation of the wave packet following electron transfer. Upon the formation of $O_2^-O_4$ by ET, the species must execute nuclear motions in order to break bonds along the ion induced-dipole coordinate corresponding to the O_2^--O_4 reaction path (Fig. 4). The ps time scale reflects the dynamics of vibrational energy transfer in the solvent evaporation process. One more consideration must be addressed. As shown in Fig. 2(c), O_2^- in our source exhibits a small amount of a hot band, reflecting a vibrational temperature as high as 800 K. If O_6^- produced in the source has a similar temperature, then the thermal averaging could in principle give the appearance of a nonexponential rise. However, this is only expected when a near barrier crossing is involved.[25]

For the two processes discussed above, it is expected that the degree of vibrational excitation in O_2^- should be somewhat different. However, we only monitor the vibrational changes in O_2^- as probed by its photoelectron-kinetic energy; the actual translational energy change in the recoil process, which can be observed in kinetic energy time of flight,[15] is not directly monitored here.

Solvation in the larger-sized clusters can be understood with the above picture in mind. The most noticeable experimental observation is the increase of both time constants with increasing cluster size, and the decrease in γ, the ratio of the amplitudes of the fast to slow components. The fast component is doubled in value for each additional solvent molecule, whereas the time constant for the slow component increases by a factor of 3 on going from O_6^- to O_8^- and then stays about the same, within the error bars, on going from O_8^- to O_{10}^-. As mentioned before, substantial vibrational cooling is observed for O_2^- from O_8^- or O_{10}^- as compared to O_6^- (from the PE spectra), which suggests that collisions between O_2^- and O_2 are effective during the reaction. Accordingly, in the case of core O_4^- dissociation resulting from electron recombination, the surrounding solvent O_2 molecules strongly influence the dissociation dynamics. This effect is visualized in terms of the kinematics of a collision with the solvent barrier (Fig. 4). The presence of a solvent barrier also explains the observation of an increase in O_4^- fragment intensity for the larger clusters [Fig. 2(b)]. On the other hand, for the slow channel, the time scale is dictated by the transfer of energy to the solvent and this evaporation-type process is relatively slow and is not surprising that it does not change dramatically upon going from O_8^- to O_{10}^-.[26]

In conclusion, the complexity of the reaction pathways for the ionic reaction of oxygen clusters is simplified by resolving in time and energy the photoelectron spectra of nascent and parent ions. We elucidate the role of electron transfer, electron recombination and nuclear motions on the femtosecond time scale. The stepwise solvation effect on reaction dynamics was also elucidated in this picture of wave packet bifurcation and solvent energy barrier. Future work will detail studies of solvation and will increase the photoelectron resolution in order to study vibrational structures near the transition state.

ACKNOWLEDGMENTS

NJK was supported by postdoctoral fellowships program from the Korea Science & Engineering Foundation (KOSEF) and by Caltech. TMB acknowledges financial support from the Alexander von Humboldt foundation and is grateful to Professor Ludger Wöste for help and support.

[1] A. W. Castlemann, Jr. and K. H. Bowen, J. Phys. Chem. **100**, 12911 (1996), and references therein.
[2] M. Nadal, S. Nandi, P. Wenthold, J. Kim, L. J. Andersen, Y. Ozaki, D. W. Boo, and W. C. Lineberger, in *Femtochemistry and Femtobiology: Ultrafast Reaction Dyanmics at Atomic-Scale Resolution: Nobel Symposium 101*, edited by V. Sundström (Imperial College Press, London, 1997), and references therein.
[3] A. H. Zewail, Angew. Chem. Int. Ed. Engl. **39**, 2586 (2000), and references therein.
[4] T. Tsukuda, M. A. Johnson, and T. Nagata, Chem. Phys. Lett. **268**, 429 (1997).
[5] M. J. DeLuca and M. A. Johnson, Chem. Phys. Lett. **162**, 445 (1989).
[6] P. Ayotte and M. A. Johnson, J. Chem. Phys. **106**, 811 (1997).
[7] L. A. Posey, M. J. DeLuca, and M. A. Johnson, Chem. Phys. Lett. **131**, 170 (1986).
[8] R. Li, K. A. Hanold, M. C. Garner, A. K. Luong, and R. E. Continetti, Faraday Discuss. **108**, 115 (1997).
[9] S. Matejcik, P. Stampfli, A. Stamatovic, P. Scheier, and T. D. Märk, J. Chem. Phys. **111**, 3548 (1999).
[10] K. Hiraoka, J. Chem. Phys. **89**, 3190 (1988).
[11] M. J. DeLuca, C.-C. Han, and M. A. Johnson, J. Chem. Phys. **93**, 268 (1990).

[12] C.-C. Han and M. A. Johnson, Chem. Phys. Lett. **189**, 460 (1992).
[13] L. Lehr, M. T. Zanni, C. Frischkorn, R. Weinkauf, and D. M. Neumark, Science **284**, 635 (1999), and references therein.
[14] G. Ganteför, S. Kraus, and W. Eberhardt, J. Electron Spectrosc. Relat. Phenom. **88**, 35 (1998).
[15] P. Y. Cheng, D. Zhong, and A. H. Zewail, J. Chem. Phys. **105**, 6216 (1996).
[16] D. Zhong, T. M. Bernhardt, and A. H. Zewail, J. Phys. Chem. A **103**, 10093 (1999).
[17] R. Weinkauf, K. Walter, C. Weickhardt, U. Boesl, and E. W. Schlag, Z. Naturforsch. **44a**, 1219 (1989).
[18] B. Ernstberger, H. Krause, A. Kiermeier, and H. J. Neusser, J. Chem. Phys. **92**, 5285 (1990).
[19] P. Kruit and F. H. Read, J. Phys. E **16**, 313 (1983).
[20] O. Cheshnovsky, S. H. Yang, C. L. Pettiette, M. J. Craycraft, and R. E. Smalley, Rev. Sci. Instrum. **58**, 2131 (1987).
[21] G. V. Chertihin and L. Andrews, J. Chem. Phys. **108**, 6404 (1998).
[22] M. Allan, K. R. Asmis, D. B. Popović, M. Stepanivić, N. J. Mason, and J. A. Davies, J. Phys. B **29**, 3487 (1996).
[23] J. A. A. Aquino, P. R. Taylor, and S. P. Walch, J. Chem. Phys. **114**, 3010 (2001).
[24] The excited O_2^- ions with $v'' \geqslant 4$ can undergo autodetachment since $v'' = 4$ state of O_2^- is higher than $v' = 0$ state of O_2 neutral. With pump pulse only, we observed the autodetachment signal of nascent O_2^- generated from the $(O_2)_n^-$ dissociation at 800 nm.
[25] N. F. Scherer and A. H. Zewail, J. Chem. Phys. **87**, 97 (1987).
[26] M. Gutmann, D. M. Willberg, and A. H. Zewail, J. Chem. Phys. **97**, 8048 (1992).